Internal sheaths in electronegative discharges

I. G. Kouznetsov, A. J. Lichtenberg, and M. A. Lieberman[a)]
Department of Electrical Engineering and Computer Sciences and the Electronics Research Laboratory, University of California, Berkeley, California 94720

(Received 29 March 1999; accepted for publication 8 June 1999)

In three component electronegative discharges a parameter regime can be found in which the positive ions reach the local ion sound velocity at a position where the negative ion density may be significant compared to the electron density. For this regime a quasineutral electronegative core breaks down and a space charge region forms. Solutions in the space charge region are obtained in collisionless and collisional cases, neglecting ionization and positive-negative ion recombination. The structure of the non-neutral region is shown to vary significantly with the ratio of the negative ion and electron densities at the core edge, the ratio of ion and electron temperatures, and the ratio of the electron Debye length to the ion mean free path. If the first ratio is not too large the non-neutral region displays potential oscillations on the electron Debye length spatial scale, which damp away on the scale of the ion–neutral mean free path. The non-neutral region then terminates within the plasma. The change in electric potential across this region is several times the negative ion temperature, which is sufficient to confine the negative ions to the core. The non-neutral region merges with a quasineutral halo containing essentially only positive ions and electrons. If the negative ion density is sufficiently high compared to the electron density the electropositive halo disappears and the non-neutral region extends from the ion sound velocity threshold to the wall. For intermediate values of the negative ion density, a space charge double layer forms between the electronegative and electropositive regions. © *1999 American Institute of Physics.* [S0021-8979(99)02418-4]

I. INTRODUCTION

Electronegative gases have found numerous applications in plasma processing. The presence of negative ions introduces several complications into discharge analysis, compared to relatively well studied electropositive discharges, such as the plasma–sheath transition and the division of the discharge into electronegative and electropositive regions. In the simplest case of an electropositive plasma, consisting of positive ions and electrons, the interaction of the plasma with an absorbing wall leads to formation of a boundary layer, a sheath, adjoining the wall. The necessary condition for the formation of a stationary sheath is expressed by Bohm's criterion[1,2] which requires that ions entering the sheath have a velocity equal to the ion sound velocity. This velocity is not achieved by ions in thermal motion. A potential difference of the order of the electron temperature is required to accelerate the ions as they move from the discharge center toward the wall.

In electronegative plasmas the ion sound velocity varies with the ratio of the negative ion and electron densities[2,3] and can be significantly reduced compared to that in an electropositive plasma. A potential difference of a few times the negative ion temperature is then sufficient for the positive ions to accelerate to the local ion sound velocity. Since the negative ion temperature is usually very small compared to the electron temperature, the small electric potential inside the bulk plasma contains the negatively charged ions but not the electrons. Thus the plasma divides into two regions: a central electronegative core containing positive ions, negative ions and electrons, and an outer halo region consisting mainly of positive ions and electrons.[4–7] The transition from the electronegative core to the electropositive halo can occur smoothly, if the local ion sound velocity is not reached within the core, or rather abruptly, if the positive ions reach the ion sound velocity inside the electronegative core. If the negative ion density at the edge of the electronegative core is high enough the electropositive halo may not exist, as discussed in the present paper.

In a previous paper[8] we solved for the discharge equilibrium, assuming that there is an abrupt transition from an electronegative to an electropositive plasma, at the position where the drift velocity reaches the local ion sound velocity. This ansatz was based on the intuition that hydrodynamic solutions either produce shocks or non-neutral regions at this transition. A small additional electric field would be sufficient to retard the negative ions, with the result being an abrupt transition to the electropositive edge region.

In this paper we investigate this ansatz by explicitly retaining the non-neutral terms in the macroscopic equations. We show that the inclusion of these terms generates the weak electric field required to confine the negative ions. In Sec. II a plasma model is introduced based on fluid equations for positive ions and Boltzmann equilibrium for negative ions and electrons. In Sec. III it is shown that the ion sound limitation leads to a space charge buildup which breaks down the quasineutral electronegative core. In Sec. IV we reproduce the model equations from our previous work which are used

a)Electronic mail: lieber@eecs.berkeley.edu

to present a general solution for the regime in which the positive ions reach the ion sound velocity in the core. The space charge region is studied in Sec. V, in collisionless and collisional cases, assuming that ionization and positive–negative ion recombination are negligible in this region. Solutions are obtained numerically for different values of the positive and negative ion temperatures. In Sec. VI theoretical solutions are compared to results of simulations. The results and limitations of the analysis are discussed in Sec. VII.

II. PLASMA HYDRODYNAMICS

In this section, a hydrodynamical model is developed which describes a three species discharge plasma, consisting of positive ions, negative ions and electrons, interacting among themselves and with a neutral gas. The plasma discharge is produced inside a cylindrical chamber. The cylinder aspect ratio is assumed to be large (length$\ll$diameter) so that a one dimensional plane parallel analysis can be applied.

The positive ion particle balance equation in a steady state can be written as

$$\frac{d\Gamma_+}{dx} = K_{\rm iz} n_0 n_e - K_{\rm rec} n_- n_+ , \tag{1}$$

where Γ_+ is the positive ion flux, n_0 is the neutral gas density, n_+, n_- and n_e are, respectively, the positive ion, negative ion and electron densities, and $K_{\rm iz}$ and $K_{\rm rec}$ are the ionization and recombination reaction rate constants. The positive ion flux is given by

$$\Gamma_+ = n_+ u_+ , \tag{2}$$

where u_+ is the average positive ion velocity.

The positive ion momentum balance equation can be written as

$$\begin{aligned} n_+ M_+ u_+ \frac{du_+}{dx} &= -eT_+ \frac{dn_+}{dx} - n_+ e \frac{d\Phi}{dx} \\ &\quad - (\nu_m n_+ + K_{\rm iz} n_0 n_e + K_{\rm rec} n_- n_+) M_+ u_+ , \end{aligned} \tag{3}$$

where M_+ and T_+ are the positive ion mass and temperature (in volts), respectively, Φ is the electric potential, and ν_m is the ion momentum transfer frequency due to collisions with neutrals. At high pressure ν_m can be regarded as a constant, $\nu_m = \overline{\nu}_+ / \lambda$, where $\overline{\nu}_+ = \sqrt{8eT_+/\pi M_+}$ is the positive ion mean thermal speed, $\lambda = 1/n_0 \sigma_{\rm mi}$ is the positive ion mean free path, and $\sigma_{\rm mi}$ is the ion momentum transfer cross section. The ion drift velocity u_+ can become larger than $\overline{\nu}_+$ at low pressure in which case the momentum transfer frequency varies with the ion velocity as $\nu_m = \pi |u_+| / 2\lambda$.[9,10] The last term on the right hand side of Eq. (3) is an effective friction force which includes three different contributions. The first arises from the ion momentum loss in collisions with neutrals. The second is due to generation of new ions which on average have zero momentum. The last is due to the positive–negative ion recombination. Assuming that the recombining positive ions are moving with the average velocity of the ion fluid u_+, then every recombining ion reduces momentum of the ion fluid by $M_+ u_+$. Thus, both ionization and recombination exert a drag force on the moving ion fluid. However, the most important part in the drag force is due to collisions with neutrals.

It is not intended here to develop a full hydrodynamic description of the three species electronegative plasma. Instead it is assumed that both negatively charged species, the electrons and negative ions, are in Boltzmann equilibrium with the electric field

$$n_e = n_{e0} \exp\left(\frac{\Phi}{T_e}\right), \tag{4}$$

$$n_- = n_{-0} \exp\left(\frac{\Phi}{T_-}\right), \tag{5}$$

where n_{e0} and n_{-0} are, respectively, the electron and negative ion densities in the center of the discharge, and T_e and T_- are the electron and negative ion temperatures, respectively. Conditions when this assumption is justified were studied in Ref. 11. The electric potential Φ is taken to be zero in the center of the discharge. Poisson's equation relates the densities of the charged species and the electric potential

$$\frac{d^2\Phi}{dx^2} = -\frac{e}{\epsilon_0}(n_+ - n_e - n_-), \tag{6}$$

where ϵ_0 is the permittivity of free space. This completes the model equations.

It is convenient[12] to introduce nondimensional position, potential, positive ion energy, and charged species density variables

$$z = \frac{x}{\lambda}, \quad \eta = -\frac{\Phi}{T_e}, \quad w_+ = \frac{M_+ u_+^2}{2eT_e}, \quad h_i = \frac{n_i}{n_{\rm es}}, \tag{7}$$

where $n_{\rm es}$ is the electron density at some position specified below, and index i denotes all charged species.

In these nondimensional variables equations (1)–(3) become

$$\frac{dj_+}{dz} = \tilde{\nu}_{\rm iz} - \tilde{\nu}_{\rm rec}, \tag{8}$$

$$j_+ = h_+ w_+^{1/2}, \tag{9}$$

$$\frac{dw_+}{dz} = -\frac{1}{\gamma_+ h_+}\frac{dh_+}{dz} + \frac{d\eta}{dz} - 2w_+ \frac{\tilde{\nu}_m + \tilde{\nu}_{\rm iz} + \tilde{\nu}_{\rm rec}}{j_+}, \tag{10}$$

where

$$\begin{aligned} j_+ &= \frac{\Gamma_+}{n_{\rm es}} \sqrt{\frac{M_+}{2eT_e}}, \quad \tilde{\nu}_m = \frac{\nu_m n_+}{n_{\rm es}} \lambda \sqrt{\frac{M_+}{2eT_e}}, \\ \tilde{\nu}_{\rm iz} &= \frac{K_{\rm iz} n_0 n_e}{n_{\rm es}} \lambda \sqrt{\frac{M_+}{2eT_e}}, \quad \tilde{\nu}_{\rm rec} = \frac{K_{\rm rec} n_- n_+}{n_{\rm es}} \lambda \sqrt{\frac{M_+}{2eT_e}}, \end{aligned} \tag{11}$$

and $\gamma_\pm = T_e / T_\pm$. The electron and negative ion densities, Eqs. (4) and (5), become

$$h_e = \frac{n_{e0}}{n_{\rm es}} \exp(-\eta), \tag{12}$$

$$h_- = \frac{n_{-0}}{n_{\rm es}} \exp(-\gamma_- \eta). \tag{13}$$

The electron temperature is usually equal to a few volts, whereas ion temperatures are only a small fraction of a volt, which means that $\gamma_{\pm} \gg 1$ in all practical cases. The Poisson's equation (6) can be written in the following form:

$$\epsilon^2 \frac{d^2\eta}{dz^2} = h_+ - h_e - h_-, \tag{14}$$

where $\lambda_D = \sqrt{\epsilon_0 T_e / e n_{es}}$ is the electron Debye length at the position such that $n_e = n_{es}$, and $\epsilon = \lambda_D / \lambda$ is a nondimensional parameter. The Debye length is normally very small compared with the ion mean free path which results in $\epsilon \ll 1$.

III. QUASINEUTRALITY BREAKDOWN AND ION SOUND LIMITATION

Logarithmic differentiation of Eq. (9) produces the following equation:

$$\frac{1}{j_+}\frac{dj_+}{dz} = \frac{1}{h_+}\frac{dh_+}{dz} + \frac{1}{2w_+}\frac{dw_+}{dz}. \tag{15}$$

Using Eq. (14) the first right hand side term can be written as

$$\frac{1}{h_+}\frac{dh_+}{dz} = \frac{1}{h_e + h_-}\frac{d(h_e + h_-)}{dz} + \epsilon^2 \frac{h_+}{h_e + h_-}\frac{d}{dz}\left(\frac{1}{h_+}\frac{d^2\eta}{dz^2}\right). \tag{16}$$

Substituting Eqs. (12) and (13) into Eq. (16) yields

$$\frac{1}{h_+}\frac{dh_+}{dz} = -\frac{1+\gamma_-\alpha}{1+\alpha}\frac{d\eta}{dz} + \epsilon^2 \frac{h_+}{h_e + h_-}\frac{d}{dz}\left(\frac{1}{h_+}\frac{d^2\eta}{dz^2}\right), \tag{17}$$

where $\alpha(z)$ is a ratio of the negative ion density to the electron density. As follows from Eqs. (12) and (13) this ratio varies with the electric potential according to

$$\alpha = \alpha_0 \exp\{-(\gamma_- - 1)\eta\}, \tag{18}$$

where $\alpha_0 = n_{-0}/n_{e0}$ is a parameter measuring the plasma electronegativity. Now, by substituting dj_+/dz from Eq. (8), dw_+/dz from Eq. (10), and dh_+/dz from Eq. (17) into Eq. (15) the following equation is obtained:

$$\left\{\left(1 - \frac{1}{2\gamma_+ w_+}\right)\frac{1+\gamma_-\alpha}{1+\alpha} - \frac{1}{2w_+}\right\}\frac{d\eta}{dz} + \frac{\tilde{\nu}_m + 2\tilde{\nu}_{iz}}{j_+} = \left(1 - \frac{1}{2\gamma_+ w_+}\right)\epsilon^2 \frac{h_+}{h_e + h_-}\frac{d}{dz}\left(\frac{1}{h_+}\frac{d^2\eta}{dz^2}\right), \tag{19}$$

which generalizes an equation derived in Ref. 12 to a plasma containing negative ions, and also allows for finite ion temperature.

The right hand side of Eq. (19) represents a contribution from finite space charge. Since $\epsilon \ll 1$ this contribution is small, if the electric potential η does not vary too fast with position z. The plasma approximation is valid in this case, and Poisson's equation can be replaced by a quasineutrality condition which is equivalent to setting $\epsilon = 0$ in Eq. (14). However, the quasineutral solution obtained by solving Eq. (19) with $\epsilon = 0$ does not always exist. Indeed, for it to exist it is necessary that the first left hand side term is negative and cancels the second term which is positive definite. This is the case near the discharge center where the positive ion kinetic energy w_+ is small so that the coefficient before the electric field $d\eta/dz$ in Eq. (19) is large and negative. Since the energy w_+ increases as the ions drift in the electric field toward the walls the coefficient before the electric field becomes smaller in absolute magnitude. Larger values of the electric field are required to cancel the second left hand side term and preserve quasineutrality. This is possible as long as the coefficient before the electric field is nonpositive, i.e.,

$$w_+ \leqslant \frac{1}{2}\left(\frac{1+\alpha}{1+\gamma_-\alpha} + \frac{1}{\gamma_+}\right). \tag{20}$$

When the ion energy satisfies Eq. (20) with the equality sign, the electric field becomes infinite. If

$$w_+ > \frac{1}{2}\left(\frac{1+\alpha}{1+\gamma_-\alpha} + \frac{1}{\gamma_+}\right), \tag{21}$$

both left hand side terms are positive, and therefore the space charge contribution must be included. This interpretation is described in Ref. 12. The transitional value of the ion energy

$$w_+ = w_{+s} \equiv \frac{1}{2}\left(\frac{1+\alpha_s}{1+\gamma_-\alpha_s} + \frac{1}{\gamma_+}\right) \tag{22}$$

corresponds to the ion velocity equal to the local ion sound velocity or the Bohm speed

$$u_B = \sqrt{\frac{eT_e}{M_+}\left(\frac{1+\alpha_s}{1+\gamma_-\alpha_s} + \frac{1}{\gamma_+}\right)}. \tag{23}$$

Here $\alpha_s = \alpha_0 \exp[-(\gamma_- - 1)\eta_s]$, and η_s is the local electric potential. Equation (23) can be easily obtained from the Bohm criterion derived in Ref. 13. For some systems the negative ion temperature can be several times larger than the positive ion temperature. The term $1/\gamma_+$ is then small and can be omitted, which results in the Bohm speed expression for electronegative gases obtained in Ref. 3.

The discharge divides into several regions depending on whether quasineutrality is satisfied. If the plasma is quasineutral the plasma approximation is valid, such that taking the space charge density equal to zero leads to a solution which closely approximates the exact solution. In a sheath, on the contrary, the finite space charge density determines the physics of the solution. Quasineutrality can also be violated inside the discharge, as will become clear in Sec. IV.

IV. ION SOUND LIMITATION IN THE QUASINEUTRAL CORE

It can be concluded from Sec. III that in a quasineutral solution, the space coordinate x has a maximum l_s. The electric field at this position becomes singular. The Bohm speed appears naturally as the critical velocity of the positive ion drift, at $x = l_s$. The critical drift velocity is a result of diffusion controlled by the ion inertia.[14] With the inertia neglected, the ion drift velocity is allowed to rise above the ion sound velocity which is not physical. The solution in this

case is cut off when the ion drift velocity becomes close to the ion sound velocity. Solutions both with and without the ion inertia were obtained in Ref. 14 for electropositive plasma. It was found that omission of the inertia term only modifies the density and potential profiles close to $x=l_s$. However, at sufficiently high pressure such that $\tilde{\nu}_m \gg \tilde{\nu}_{\rm iz}$ the two solutions become virtually identical. This approximation is extended here to the electronegative plasma.

Neglecting the inertial term on the left hand side of the positive ion momentum balance equation (3) and similar terms in the momentum balance equations for the negative ions and electrons produces flux equations

$$\Gamma_i = -D_i \frac{dn_i}{dx} \pm n_i \mu_i E, \tag{24}$$

where $D_i = eT_i/m_i\nu_i$, $\mu_i = e/m_i\nu_i$ are the diffusion coefficient and mobility of species i, ν_i is the total momentum transfer collision frequency, E is the electric field, and the $\pm$ corresponds to positive and negative carriers, respectively. In a steady state, the electric currents must balance and, when Eq. (20) is satisfied, Poisson's equation (6) can be replaced by charge neutrality.

Using these conditions, the Boltzmann distributions for the electrons Eq. (4) and negative ions Eq. (5), and the Einstein relations, the positive ion flux can be written as

$$\Gamma_+ = -D_{a+} \frac{dn_+}{dx}, \tag{25}$$

where D_{a+} is the ambipolar diffusion coefficient for the positive ions[7,8,15]

$$D_{a+} \simeq D_+ \frac{1+\gamma_+ + (\gamma_+ + \gamma_-)\alpha}{1+\gamma_- \alpha}. \tag{26}$$

From Eq. (26), we see that for $\alpha \gg 1$ we have $D_{a+} \simeq D_+(1+T_-/T_+)$ which we shall assume to hold over the electronegative plasma core, until the ion sound transition.

For $\gamma_- \gg 1$, $n_e \simeq n_{e0}$, and the positive ion particle balance equation (1) becomes

$$\frac{d}{dx}\left(-D_{a+}\frac{dn_+}{dx}\right) = K_{\rm iz} n_0 n_{e0} - K_{\rm rec} n_- n_+ . \tag{27}$$

If the flow dominates the recombination the second right hand side term is small. Assuming that D_{a+} is constant, Eq. (27) can then be approximated by a parabolic solution[7]

$$\frac{n_+}{n_{e0}} = \frac{n_-}{n_{e0}} + 1 = \alpha_0\left(1 - \frac{x^2}{l^2}\right) + 1, \tag{28}$$

where l is the scale length of the parabola. In the previous work[7,8] this parabolic solution is used to determine the discharge plasma parameters T_e, α_0, and l, given the appropriate boundary conditions.

As the positive ions drift from the plasma center toward the walls their velocity increases and can eventually reach the ion sound velocity, Eq. (23), at some position $x=l_s$. It is assumed that the ratio of the negative ion density to the electron density, at this position, $\alpha_s \gg 1$ so that $D_{a+} \simeq D_+(1+T_-/T_+)$, a constant. A numerical model of an oxygen discharge at low pressure[8] supports this assumption.

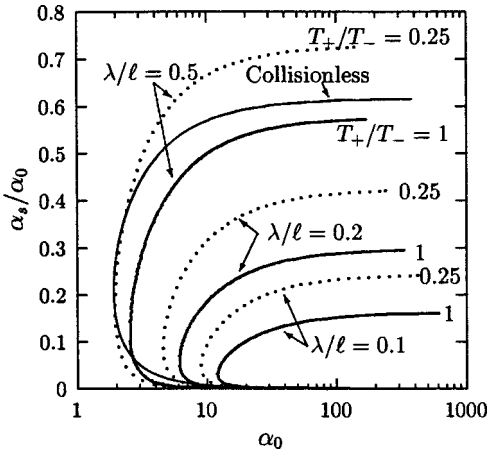

FIG. 1. The ratio α_s/α_0 vs α_0 from Eq. (31) for values of $\lambda/l = 0.1$, 0.2, and 0.5 and values of $T_+/T_- = 0.25$ (dotted lines) and 1 (solid lines). Also represented is the collisionless case (Ref. 3) with $\gamma_- = 30$.

Thus, the quasineutral parabolic solution extends over the interval $0<x<l_s$. Then at $x=l_s$, the positive ion flux, Eq. (25) is

$$-D_{a+}\frac{dn_+}{dx}\Big|_{x=l_s} = n_+(l_s)u_B, \tag{29}$$

with u_B given by Eq. (23). Substituting Eq. (28) and $D_{a+} = D_+(1+T_-/T_+)$ into Eq. (29) gives

$$D_+\left(1+\frac{T_-}{T_+}\right)\alpha_0 n_{e0}\frac{2l_s}{l^2} = (\alpha_s+1)n_{e0}u_B(\alpha_s), \tag{30}$$

where $\alpha_s = \alpha_0(1-l_s^2/l^2)$ within the parabolic approximation. Substituting Eq. (23) and $D_+ = (\pi/8)\overline{\nu}_+\lambda$ into Eq. (30), neglecting the small term $1/\gamma_-$, and then squaring both sides of the equation results in

$$\frac{\pi\lambda^2}{2l^2}\left(2+\frac{T_-}{T_+}+\frac{T_+}{T_-}\right)\alpha_0(\alpha_0-\alpha_s)\alpha_s = (\alpha_s+1)^3 + \frac{T_+}{T_-}\alpha_s(\alpha_s+1)^2. \tag{31}$$

Provided α_0 is known, this equation can be solved numerically for α_s. In Fig. 1, the ratio α_s/α_0 is plotted versus α_0 for values of $\lambda/l = 0.1$, 0.2, 0.5 and for values of $T_+/T_- = 1$ and 0.25. Since Eq. (31) is obtained assuming $n_e \simeq n_{e0}$, it cannot be extended to purely electropositive plasmas in which case $\alpha_0 = 0$. Equation (31) applies to considerably electronegative plasmas with $\alpha_0 > 1$, as is also seen in Fig. 1. In our previous work[8] we investigated this transition only for $T_+/T_- = 1$. However, particle-in-cell (PIC) simulations of electronegative plasmas indicate that the spatially averaged value of $T_+/T_- \leqslant 1$, such that we present solutions that bound this value. For comparison, the ratio α_s/α_0 obtained from collisionless theory,[3,16] is shown in the same figure. The collisionless curve is for $\gamma_- = 30$, but depends weakly on γ_- for $\gamma_- > 30$. The collisional model developed in the present work, which is for large $\gamma_\pm$, approximately matches the collisionless curve for $\lambda/l = 0.5$.

Equation (31) has no real solutions for small α_0, which means that the ion sound velocity is not reached inside the

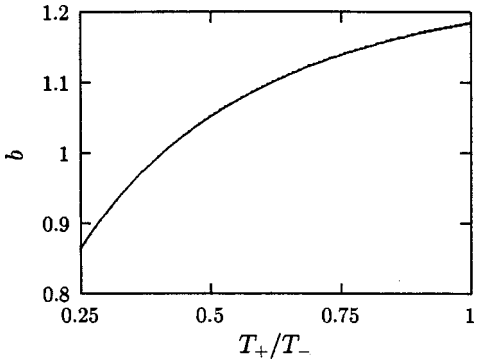

FIG. 2. Values of b vs T_+/T_-.

electronegative region. For larger α_0 Eq. (31) has two positive solutions, with the solution with the smaller value of l_s/l (larger value of α_s) giving the position where the quasineutrality breaks down, as has also been noted in a somewhat different context in Ref. 16. At the onset of the ion sound limitation, when Eq. (31) has a single solution, we find in the limit of $\lambda/l \ll 1$ a critical value of α_0,

$$\alpha_{0\mathrm{cr}} = \frac{l}{\lambda} b(T_+/T_-), \tag{32}$$

where b versus the ratio of the positive to negative ion temperature is shown in Fig. 2. When the ratio T_+/T_- varies from 0.25 to 1, b increases slowly from 0.85 to 1.2. If $\alpha_0 \geqslant \alpha_{0\mathrm{cr}}$ the quasineutral electronegative core ends at $x=l_s$, and extending the solution further requires a non-neutral region which is considered in Sec. V.

V. SPACE CHARGE REGION

When Eq. (21) applies both left hand side terms in Eq. (19) are positive. Therefore the space charge contribution which appears on the right hand side of Eq. (19) must be of the same order of magnitude as any of the left hand side terms. Comparing the first left hand side term to the right hand side term leads to $d\eta/dz \sim \epsilon^2 d^3\eta/dz^3$. This means that the characteristic length inside the space charge region is determined by the electron Debye length λ_D rather than the ion mean free path λ. It is reasonable then to switch to a new nondimensional position variable

$$\zeta = \frac{z}{\epsilon} = \frac{x}{\lambda_D}. \tag{33}$$

It is convenient to shift the origin of the electric potential from the plasma center to the beginning of the space charge region, $\zeta = \zeta_s \equiv l_s/\lambda_D$. The new electric potential is then

$$\varphi = \eta - \eta_s. \tag{34}$$

Defining n_{es}, introduced in Eq. (7), as the electron density at $\zeta=\zeta_s$ leads to the nondimensional electron density $h_e=1$ in the beginning of the charge region. With ζ as the position variable, Eqs. (8), (10), and (14) become

$$\frac{dj_+}{d\zeta} = \epsilon(\tilde{\nu}_{\mathrm{iz}} - \tilde{\nu}_{\mathrm{rec}}), \tag{35}$$

$$\frac{dw_+}{d\zeta} = -\frac{1}{\gamma_+ h_+}\frac{dh_+}{d\zeta} + \frac{d\varphi}{d\zeta} - 2\epsilon w_+ \frac{\tilde{\nu}_m + \tilde{\nu}_{\mathrm{iz}} + \tilde{\nu}_{\mathrm{rec}}}{j_+}, \tag{36}$$

$$\frac{d^2\varphi}{d\zeta^2} = h_+ - h_e - h_-. \tag{37}$$

The electron and negative ion densities, Eqs. (12) and (13), can then be written as

$$h_e = \exp(-\varphi), \tag{38}$$

$$h_- = \alpha_s \exp(-\gamma_-\varphi). \tag{39}$$

Since $\epsilon \ll 1$ the momentum transfer, ionization and recombination would appear to play a relatively minor role in the space charge region. As a first approximation, the collisionless case corresponding to $\epsilon=0$ is considered in Sec. V A.

A. Collisionless case

Although it is necessary to include collisions to determine the transition behavior, some insight is gained by first considering the collisionless limit. Integration of Eqs. (35) and (36) with $\epsilon=0$ produces the positive ion continuity and energy balance equations in the form

$$j_+ \equiv h_+ w_+^{1/2} = h_{+s} w_{+s}^{1/2}, \tag{40}$$

$$w_+ = w_{+s} - \frac{1}{\gamma_+}\ln\left(\frac{h_+}{h_{+s}}\right) + \varphi, \tag{41}$$

where $h_{+s} = 1+\alpha_s$, the positive ion density at $\zeta=\zeta_s$, and w_{+s}, the positive ion energy, is obtained from Eq. (22). Using Eq. (40) the positive ion density can be written as

$$h_+ = (1+\alpha_s)\left(\frac{w_{+s}}{w_+}\right)^{1/2}. \tag{42}$$

Substituting Eq. (42) into Eq. (41) yields

$$w_+ = w_{+s} + \frac{1}{2\gamma_+}\ln\left(\frac{w_+}{w_{+s}}\right) + \varphi, \tag{43}$$

which relates the positive ion energy and the electric potential.

Substitution of Eqs. (38), (39), and (42) into Poisson's equation (37) yields

$$\frac{d^2\varphi}{d\zeta^2} = h_\rho(\varphi) \equiv -\frac{dV(\varphi)}{d\varphi}, \tag{44}$$

where

$$h_\rho(\varphi) = (1+\alpha_s)\left(\frac{w_{+s}}{w_+}\right)^{1/2} - \exp(-\varphi) - \alpha_s \exp(-\gamma_-\varphi) \tag{45}$$

is the nondimensional space charge density and

$$V(\varphi) = 1 - \exp(-\varphi) + \frac{\alpha_s}{\gamma_-}\{1-\exp(-\gamma_-\varphi)\} - 2(1+\alpha_s)w_{+s}^{1/2}\left\{w_+^{1/2} - w_{+s}^{1/2} + \frac{1}{2\gamma_+ w_+^{1/2}} - \frac{1}{2\gamma_+ w_{+s}^{1/2}}\right\} \tag{46}$$

with $w_+(\varphi)$ obtained from Eq. (43).

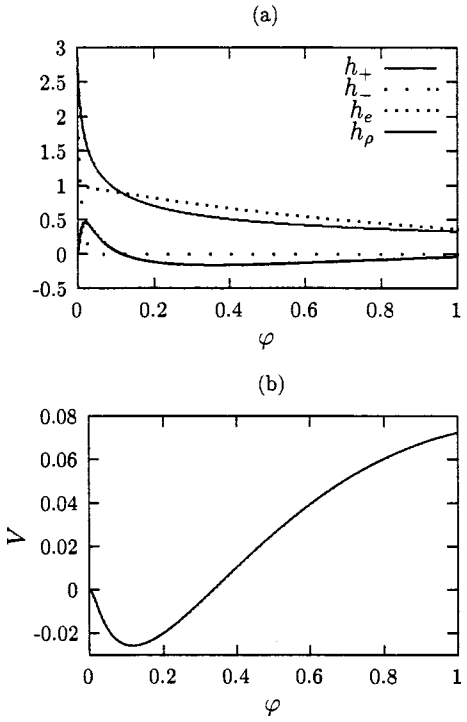

FIG. 3. Collisionless case with $\gamma_\pm = 100$ and $\alpha_s = 2$. (a) Particle densities of the positive ions h_+, negative ions h_-, and electrons h_e and the charge density h_ρ inside the space charge region versus the electric potential. (b) The quasipotential $V(\varphi)$ which satisfies Eq. (46).

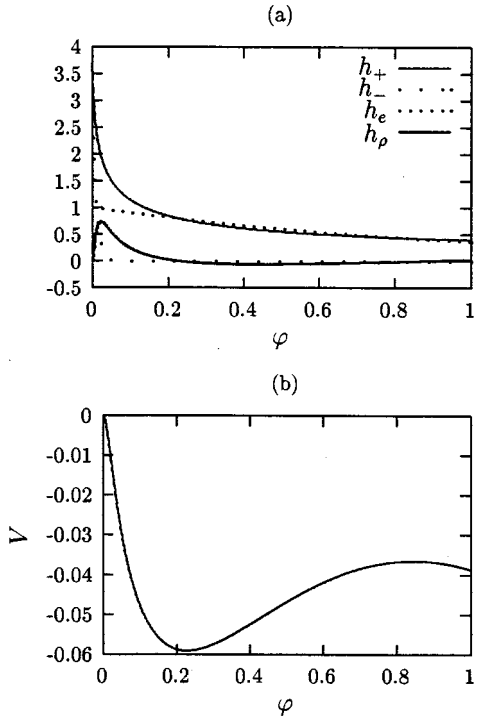

FIG. 4. The same as Fig. 3 with $\gamma_\pm = 100$ and $\alpha_s = 2.7$.

Equation (44) is known from the theory of ion acoustic shock waves, where $V(\varphi)$ has an expression different from Eq. (46).[17] Nonetheless, a regime can be found in which $V(\varphi)$ from Eq. (46) has the shape of $V(\varphi)$ in the ion acoustic shock wave, as is shown below. The behavior of the solution of Eq. (44) can be studied using an analogy to a particle moving in a potential field.[17] The motion of a particle subjected to a force $-m dV(x)/dx$ is governed by the equation:

$$\frac{d^2x}{dt^2} = -\frac{dV(x)}{dx}.$$

Equation (44) is the same as that of a particle, with the potential φ replacing x, ζ replacing t and the quasipotential $V(\varphi)$ replacing $V(x)$.

In order to explore three different regimes of the ion sound limitation the particle densities, Eqs. (38), (39), (42), the charge density, Eq. (45), and the quasipotential, Eq. (46), are plotted in Figs. 3–5 versus the potential φ for $\gamma_\pm = 100$ and values of $\alpha_s = 2$, 2.7, and 3.5, respectively. These values are typical for an intermediate range of electronegativities.[8] As is seen in Figs. 3(a)–5(a), the negative ion density decays rapidly into the space charge region and becomes negligible after the potential increases by a few ion temperatures T_-. The positive ion density decreases much more slowly than the negative ion density, which allows the space charge to form. The positive and negative ions behave in this situation just like, respectively, the positive ions and electrons do in a sheath separating a simple electropositive plasma from a wall. With this analogy in mind, this non-neutral region can be called an electronegative sheath. However, the electron density in the sheath remains essentially uniform due to the large ratio of the electron and ion temperatures. Depending on the value of α_s, the space charge density may eventually return to its original zero value, when the positive ion density matches the electron density. The charge density then may become negative if the potential continues to increase, as shown in Figs. 3(a) and 4(a). In the larger α_s case shown in Fig. 5(a), the charge density never returns to zero, so this

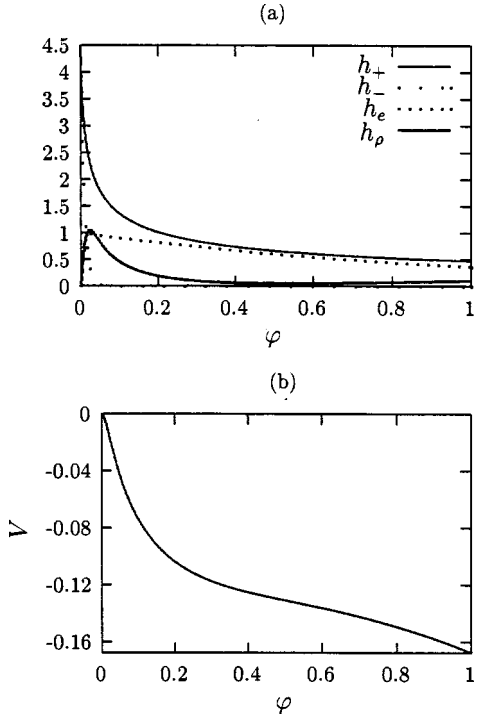

FIG. 5. The same as Fig. 3 with $\gamma_\pm = 100$ and $\alpha_s = 3.5$.

positive charge region is the only layer between the quasineutral electronegative core and the wall. This regime of the ion sound limitation is called here the positive charge regime.

The quasipotential V plotted in Figs. 3(b)–5(b) varies with φ nonmonotonically: the initial decrease is followed by a growth which may eventually take V to positive values, if α_s is sufficiently small. The case when V becomes positive for $\varphi>0$ is shown in Fig. 3(b). If the quasipotential well in Fig. 3(b) were a real well, a particle entering from the left ($x=0$) will be reflected at the right-hand side of the well ($x>0$) and return to $x=0$. In this analogy, a quasiparticle transits the quasiwell once from $\varphi=0$ to $\varphi>0$ and returns to $\varphi=0$, forming a solitary φ-potential pulse.[17] If a particle experiences a collision and loses some of its momentum while in the well, it does not return to $x=0$ but oscillates in time about the value of x at the bottom of the well. Similarly, some dissipation causes the potential φ to oscillate in space about some value of $\varphi>0$.[17] We refer here to this regime as the oscillation regime, and the oscillations are demonstrated in the collisional case considered in the following section. In the larger α_s cases shown in Figs. 4(b) and 5(b), V is negative for all $\varphi>0$. In this regime the quasiparticle is not reflected, and the potential φ rises until the chamber wall is reached. In the regime represented in Fig. 4, the space charge density is positive in the beginning of the charge region, then becomes negative, and finally returns to positive values near the wall. This regime is called here the charge double layer regime.

Boundaries separating these regimes can be determined as follows. At the transition between the charge double layer and positive charge regimes both the space charge density h_ρ and its derivative $dh_\rho/d\varphi$ become zero at the same value of φ. It is then straightforward to find that $w_+=0.5(1+1/\gamma_+)$. Substituting this into Eq. (45) with $h_\rho=0$ leads to an equation involving α_s and $\gamma_\pm$. This equation is solved numerically for α_s as a function of $\gamma_\pm$. The result is shown in Fig. 6 as a solid line where γ_- varies in the wide range from 20 to 200, and $\gamma_+/\gamma_-=1$ and 4. At the transition between the oscillation and double layer regimes V and $dV/d\varphi=-h_\rho$ become zero simultaneously at some φ. Solving Eq. (45) with $h_\rho=0$ and Eq. (46) with $V=0$ yields α_s vs $\gamma_\pm$ which is shown in Fig. 6 as a dashed line. In the positive charge regime, the charge density is large for $\varphi>0$, so the quasineutral electropositive region cannot form in this regime.

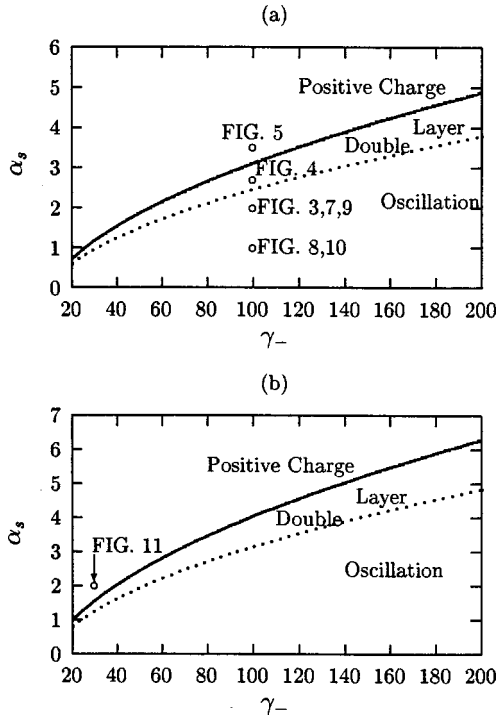

FIG. 6. Ion sound limitation regimes for (a) $T_+=T_-$ and (b) $T_+=0.25T_-$.

B. Collisional case

In this section, the parameter $\epsilon=\lambda_D/\lambda$ is assumed to be small, but finite. The ionization and recombination processes are considered unimportant in order to simplify the analysis. We shall discuss the validity of this approximation in Sec. VII. Substituting the ion momentum transfer collision frequency at low pressure, $\nu_m=\pi|u_+|/2\lambda$, and $\nu_{iz}=\nu_{rec}=0$ into Eq. (11) results in

$$\tilde{\nu}_m=\frac{\pi}{2}j_+. \tag{47}$$

Integrating Eq. (35) yields the positive ion continuity equation Eq. (40) obtained earlier. Then, the positive ion density is given by Eq. (42). Substituting Eqs. (47) and (42) into the momentum conservation equation (36) yields

$$\frac{dw_+}{d\zeta}=\frac{1}{2\gamma_+ w_+}\frac{dw_+}{d\zeta}+\frac{d\varphi}{d\zeta}-\epsilon\pi w_+. \tag{48}$$

The set of differential equations is Eq. (48) and Poisson's equation (37), with the positive and negative ion and electron densities obtained from Eqs. (42), (39), and (38).

The set is too complicated to be solved analytically. Applying the technique used in the collisionless case, one finds that collisions contribute an extra term to V from Eq. (46),

$$\delta V=-\epsilon\pi(1+\alpha_s)w_{+s}^{1/2}\int_{\zeta_s}^{\zeta}w_+^{1/2}\,d\zeta. \tag{49}$$

This contribution is negative definite and grows in magnitude with ζ which resists formation of the right-hand side slope of the quasiwell and V reaching positive values for $\zeta>\zeta_s$. It is expected then that the size of the oscillation regime in Fig. 6 decreases with increasing ϵ. As a result, the dashed curves in Fig. 6 in the collisional case are located below the collisionless dashed curves. Similarly, the solid curves, which divide the parameter space between the regions where $h_\rho\geqslant 0$ from the regions where h_ρ changes sign, are located at lower α_s in the collisional case.

The space charge region is preceded by the quasineutral electronegative core in which Poisson's equation (37) can be replaced with the plasma approximation $h_+=h_e+h_-$. This allows one to obtain a quasineutral analytical solution given by

$$w_+ = w_{+s}\left(\frac{1+\alpha_s}{\exp(-\varphi)+\alpha_s\exp(-\gamma_-\varphi)}\right)^2,$$

$$\zeta-\zeta_s=\frac{2}{\epsilon\pi}\ln\left(\frac{\exp(-\varphi)+\alpha_s\exp(-\gamma_-\varphi)}{1+\alpha_s}\right)+\frac{1}{2\epsilon\pi w_{+s}(1+\alpha_s)^2}\left[1-\exp(-2\varphi)+\frac{4\alpha_s}{\gamma_-+1}\{1-\exp(-(\gamma_-+1)\varphi)\}+\frac{\alpha_s^2}{\gamma_-}\{1-\exp(-2\gamma_-\varphi)\}+\frac{1}{\gamma_+}\{(1+\alpha_s)^2-(\exp(-\varphi)+\alpha_s\exp(-\gamma_-\varphi))^2\}\right]. \quad (50)$$

The boundary conditions used in Eq. (50) are such that at $\zeta=\zeta_s$, the position of the ion sound velocity threshold $w_+=w_{+s}$ and $\varphi=0$. This solution results in an electric field $d\varphi/d\zeta$ which becomes singular at $\zeta=\zeta_s$, but we avoid this singularity by using boundary conditions for the non-neutral region that are at $\zeta<\zeta_s$.

As in Ref. 18, we start solving the system of differential equations (37) and (48) at some position $\zeta_0<\zeta_s$, where the quasineutral solution, Eq. (50), approximately holds. The boundary conditions for w_+ and φ at $\zeta=\zeta_0$ are obtained from Eq. (50), and the boundary condition for $d\varphi/d\zeta$ is obtained by differentiating Eq. (50). As demonstrated in Ref. 18, this way of setting up the boundary conditions does not produce artificial oscillations, when Eqs. (37) and (48) are integrated numerically. Numerical solution is obtained using a Runge–Kutta–Fehlberg algorithm.[19]

First, the solution for values of $\gamma_\pm=100$, $\alpha_s=2$, and $\epsilon=0.01$ is studied. These parameters fall into the oscillation regime in Fig. 6(a), according to the collisionless theory. The potential φ versus ζ is plotted in Fig. 7(a). Similarity in the potential variation in the collisional and collisionless cases in the beginning of the space charge region is apparent. In the collisional case, however, the potential doesn't return to zero after passing through the maximum. Instead, it experiences nonlinear oscillations with a spatial period on the order on λ_D. The oscillations begin at $\zeta=\zeta_s$, the point of the ion sound velocity threshold, and not at the point where the calculation begins, at $\zeta=\zeta_s-5$. Therefore, the boundary conditions are set correctly, and the oscillations are caused by the ion sound velocity threshold. The oscillations are dissipated over a distance on the order of the ion mean free path λ. Apart from oscillations, the potential also increases on average over a distance on the order of λ, and it grows exponentially inside the wall sheath. In the case considered $\lambda/\lambda_D=100$, which corresponds, for example, to an oxygen discharge at 2.6 mTorr with the electron density $n_{es}=10^{16}\,\mathrm{m}^{-3}$. We use the ion momentum transfer cross section $\sigma_{mi}=10^{-18}\,\mathrm{m}^2$ in the calculation of λ and assume that the ions are at room temperature.

The particle densities and the space charge density h_ρ versus ζ are shown in Fig. 7(b). The following observations can be made. The boundary conditions which match the non-

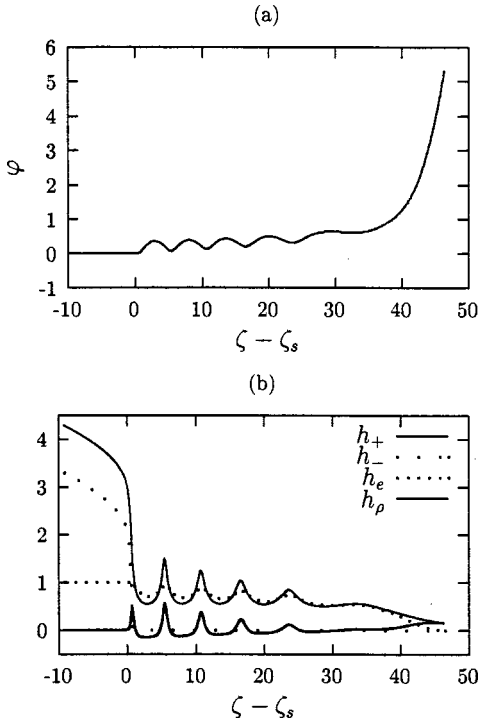

FIG. 7. Collisional case with $\gamma_\pm=100$, $\lambda/\lambda_D=100$, and $\alpha_s=2$. (a) The electric potential vs the position ζ. (b) Particle densities of the positive ions h_+, negative ions h_-, and electrons h_e and the charge density h_ρ vs the position ζ.

neutral to the quasineutral solutions imply that $h_\rho=0$ at the boundary. Although the quasineutrality is not assumed at any other position the charge density is negligibly small for $\zeta<\zeta_s$, i.e., until the positive ions reach the ion sound velocity. This justifies using the quasineutral solution to construct the boundary conditions for the non-neutral solution which is done here. The negative ion density is seen to drop to zero on the order of λ_D. The positive ion density experiences oscillations about the electron density with a spatial period of a few λ_D. The oscillation amplitude decays over a length on the order of λ. These oscillations have also been observed in rf discharge simulations using a fluid description of the ions coupled to a Monte Carlo simulation of the electrons.[20] The electron density is less affected by the electric potential variation, because of the high electron temperature. The space charge density in the non-neutral region is seen to oscillate about zero. The oscillation amplitude diminishes considerably, but it does not become negligible until the regular sheath starts to form at about $\zeta\simeq\zeta_s+30$. The charge density approaching zero can signal a transition to another quasineutral region downstream of the space charge region.

The new quasineutral region is clearly seen in Fig. 8 in which case $\alpha_s=1$ and the other parameters are the same. Now, there is sufficient space between the position of the ion sound velocity threshold and the wall, so that a quasineutral region forms which contains only the positive ions and electrons. The non-neutral region can be called an internal sheath in this case. It separates two quasineutral regions: the electronegative core and the electropositive halo. If there is no additional ionization in the halo, which has been assumed here, then from the charge density h_ρ the electropositive halo

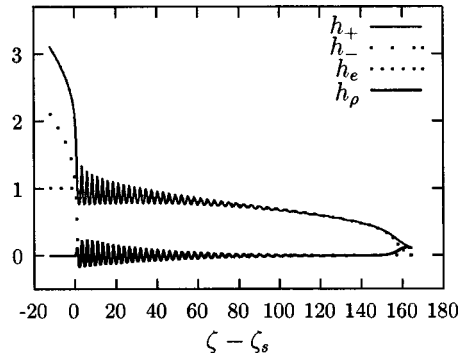

FIG. 8. The same as Fig. 7(b) with $\gamma_\pm = 100$, $\lambda/\lambda_D = 100$, and $\alpha_s = 1$.

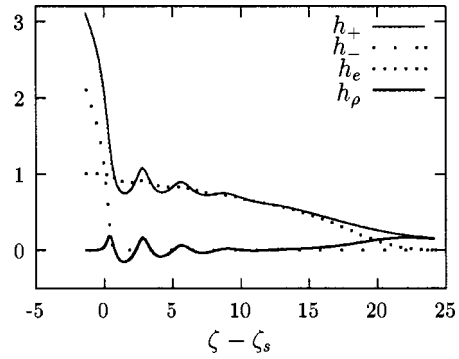

FIG. 10. The same as Fig. 7(b) with $\gamma_\pm = 100$, $\lambda/\lambda_D = 10$, and $\alpha_s = 1$.

is found to be about $\lambda/2$ long, and it merges around $\zeta \simeq \zeta_s + 150$ with the regular wall sheath.

When ϵ is increased to 0.1 the size of the oscillation regime decreases so that the parameters $\alpha_s = 2$ and $\gamma_\pm = 100$ fall into the expanding double layer regime, as is seen in Fig. 9. The potential φ, shown in Fig. 9(a), increases monotonically with position ζ. Observing the variation of the charge density shown in Fig. 9(b), one can see the familiar double layer structure. The collisionless case provides a guideline for moving into the oscillation regime, which is to reduce α_s, as seen in Fig. 6. The collisional case, with $\alpha_s = 1$, is shown in Fig. 10, giving an oscillatory solution and a return to quasineutrality. In the cases shown in Figs. 9 and 10 $\lambda/\lambda_D = 10$, which corresponds to an oxygen discharge at 26 mTorr and $n_{es} = 10^{16}\,\mathrm{m}^{-3}$.

To observe the ion sound limitation regime without a double layer, we take $\alpha_s = 2$, $\gamma_- = 30$, $\gamma_+ = 120$, and $\epsilon = 0.1$ with the solution presented in Fig. 11. As follows from Fig. 6(b), these parameters lie inside the positive charge regime.

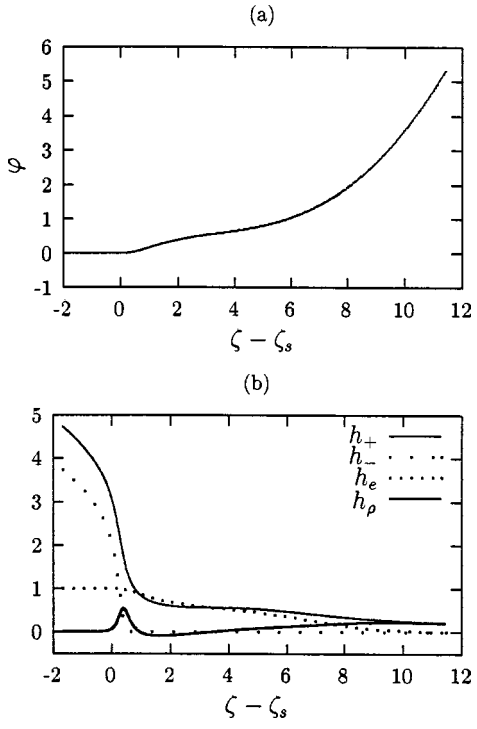

FIG. 9. The same as Fig. 7 with $\gamma_\pm = 100$, $\lambda/\lambda_D = 10$, and $\alpha_s = 2$.

VI. PARTICLE-IN-CELL SIMULATION RESULTS

The analytic theory of the ion sound limitation regimes presented in the previous sections is compared with PIC simulations. The simulations were done using the PDP1 code which includes the most important collisional processes using Monte Carlo methods.[21]

The standard PDP1 code was modified in two ways. First, the positive and negative ion masses were reduced in the simulation to $60m_e$ and $30m_e$, respectively. This significantly increases simulation speed, which is very desirable, since a long run time is required to average out the noise in the space charge density. Reducing the ion mass affects reaction rate constants, which are given by[22]

$$K(T_{\mathrm{eff}}) = \frac{2}{eT_{\mathrm{eff}}}\left(\frac{2}{\pi m_R e T_{\mathrm{eff}}}\right)^{1/2} \times \int_0^\infty \sigma_R(\mathcal{E}_R)\exp\left(-\frac{\mathcal{E}_R}{eT_{\mathrm{eff}}}\right)\mathcal{E}_R\, d\mathcal{E}_R,$$

where $m_R = m_1 m_2/(m_1 + m_2)$ is the reduced mass of the colliding particles, T_{eff} is an effective temperature, σ_R is a reaction (collision) cross section, $\mathcal{E}_R$ is the collision energy, and it is assumed that colliding species have Maxwellian distributions. For electron collisions with heavy particles $m_R \simeq m_e$ and $T_{\mathrm{eff}} \simeq T_e$. For collisions of heavy particles among themselves $m_R \sim M$, the positive or negative ion

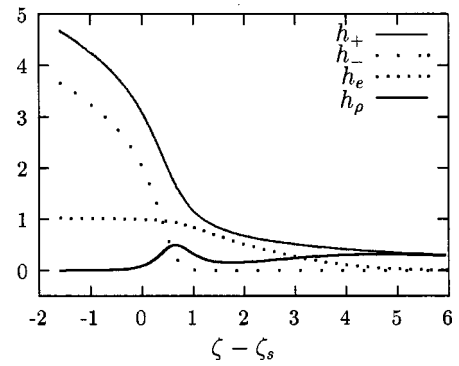

FIG. 11. The same as Fig. 7(b) with $\gamma_+ = 120$, $\gamma_- = 30$, $\lambda/\lambda_D = 10$, and $\alpha_s = 2$.

mass, and $T_{\text{eff}} \sim T_i$, the ion temperature. Then, reducing the ion mass leaves rate constants for the electron–heavy particle reactions (collisions) unchanged, while increasing rate constants for the heavy particle collisions among themselves by $f=(M_{\text{real}}/M_{\text{new}})^{1/2}$ times. The ion diffusion coefficient is also increased by the same factor. If cross sections for the electron–heavy particle collisions all also increased by f times all rate constants then the ion diffusion coefficients will be increased by the same factor of f. In this case, the simulation with the reduced ion mass is expected to give results close to those of the simulation with the real ion mass. For a discharge in oxygen $f=31.3$.

Second, an alternative electron heating mechanism is built into the code to transfer power to the plasma. In the standard code the discharge is sustained capacitively, by driving the plasma with the voltage or current source at the plates. This results in oscillating, high voltage sheaths near the plates. Now, the change in the electric potential across the structures described above is only several times the negative ion temperature. This potential change and the space charge density variation associated with it might go undetected, if an oscillating, high voltage sheath is nearby. In the simulation, both plates were grounded, and the electrons were subject to a 13.56 MHz spatially uniform electric field, parallel to the plates. The direction along the plates is not resolved in the 1D3v code which accounts for one spatial dimension and three velocity components. A nearly isotropic electron velocity distribution was obtained due to electron scattering. Because the electric field was directed along the plates and the plates were grounded, the sheaths near the plates were stationary, low voltage sheaths. This electron heating mechanism is essentially a simple model of an inductive source operation in which power transferred to the electrons is primarily determined by the rf azimuthal electric field.[2,23] With a constant rf electric field source, the simulation is unstable: work done on the electrons by the electric field over an rf cycle is proportional to the electron number, as opposed to being a constant. This problem was resolved by tuning the electric field amplitude so that the number of electrons in the simulation matches the constant electron number given in the input deck. The tuning was done automatically by a fuzzy logic controller introduced into the code. The controller uses the electron number and its time derivative as input parameters and the electric field amplitude as the control parameter. The details of the controller are given in Ref. 24.

Numerical results for the case of an oxygen discharge at $p=5$ mTorr ($n_0=1.6\times10^{20}\,\text{m}^{-3}$) and $n_{e0}=2.66\times10^{15}\,\text{m}^{-3}$ are shown in Fig. 12. The plate spacing was 3.6 cm. Figure 12(a) shows the positive and negative ion and electron temperatures versus the position. At the discharge center, $T_e=4.07$ eV, $T_-=0.078$ eV and $T_+=0.027$ eV (313 K), so that $\gamma_-=52$ and $\gamma_+=151$. The electron temperature is essentially constant throughout the discharge, but the negative ion temperature increases by an order of magnitude during transition from the electronegative core to the electropositive halo region. The electropositive region length in this case is comparable to the ion mean free path $\lambda=0.6$ cm, as is seen in Fig. 12(b). The negative ion profile in the electronegative

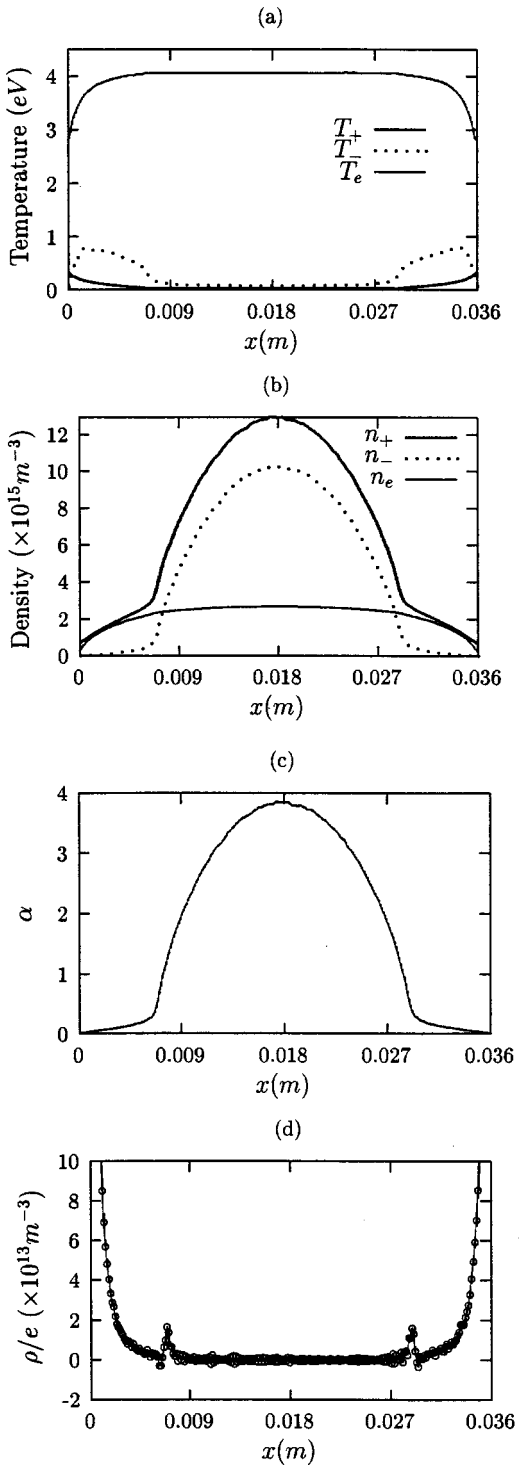

FIG. 12. Simulation results of an rf discharge in oxygen at $p=5$ mTorr and $n_{e0}=2.66\times10^{15}\,\text{m}^{-3}$. (a) The positive and negative ion and electron temperatures. (b) The positive and negative ion and electron densities. (c) The ratio of the negative ion to electron density. (d) The space charge density divided by the unit charge.

core approximately follows a parabola with $l=1.2$ cm. Then, $\lambda/l=0.5$. The space charge double layers separating the electronegative core from two electropositive halo regions are clearly seen in Fig. 12(d). The quasineutrality in the core region breaks at $\alpha_s \simeq 1$, as seen from Fig. 12(c). The point with coordinates $\alpha_s/\alpha_0=0.26$, $\alpha_0=3.8$ lies close to

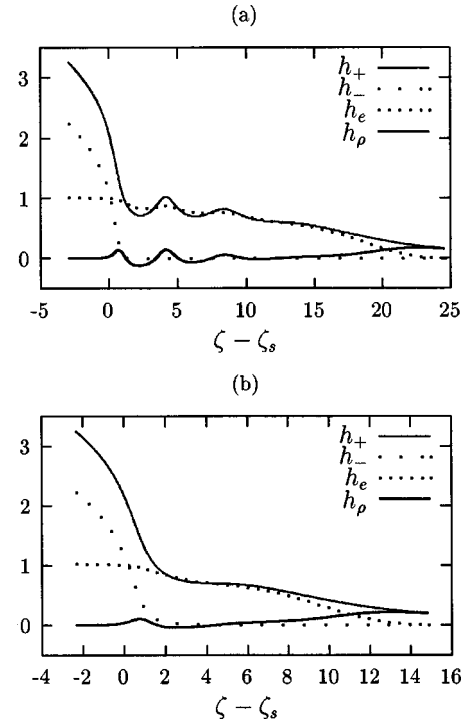

FIG. 13. The structure of the space charge region as predicted by the theoretical model with the parameters obtained from the simulation results in Fig. 12. (a) The negative ion distribution with one Boltzmann class, $\alpha_s = 1$, $\gamma_- = 52$, $\gamma_+ = 151$ and $\epsilon = 0.05$. (b) The negative ion distribution with two Boltzmann classes, $\alpha_s^{(c)} = 0.7$, $\gamma_-^{(c)} = 40$, $\alpha_s^{(h)} = 0.3$, $\gamma_-^{(h)} = 10$, $\gamma_+ = 151$, and $\epsilon = 0.05$.

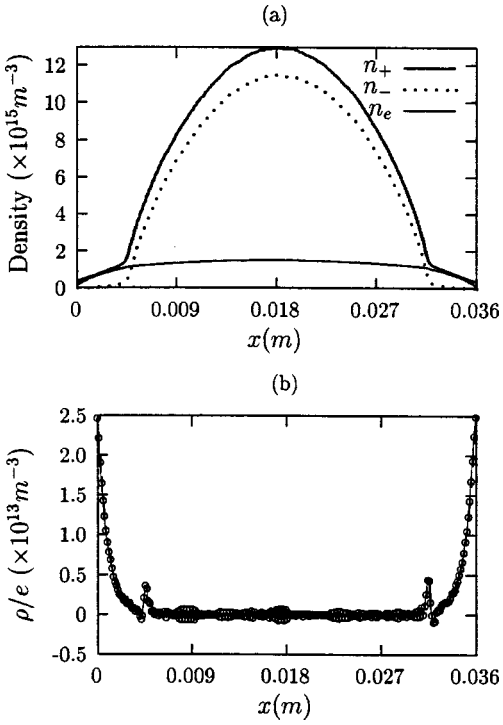

FIG. 14. Simulation results of an rf discharge in oxygen at $p = 10$ mTorr and $n_{e0} = 1.5 \times 10^{15}\,\mathrm{m}^{-3}$. (a) The positive and negative ion and electron densities. (b) The space charge density divided by the unit charge.

the $\lambda/l = 0.5$ curve in Fig. 1. The electron density at the position where the quasineutrality breaks, $n_{es} = 2.37 \times 10^{15}\,\mathrm{m}^{-3}$, is obtained from Fig. 12(b). The electron Debye length at this position is $\lambda_D = 0.03\,\mathrm{cm}$, so that $\epsilon = \lambda_D/\lambda = 0.05$. The results of the theoretical model with the values of α_s, γ_-, γ_+ and ϵ obtained above from the simulation are shown in Fig. 13(a). The space charge density exhibits only three oscillation cycles about zero. This result marginally disagrees with the simulation. The theoretical model can be better matched to the simulation, if the negative ion temperature increase in the halo region is accounted for. The negative ion distribution at the ion sound velocity threshold is approximated with two Boltzmann classes: (i) cold ions with $T_-^{(c)} = 0.1\,\mathrm{eV}$ and $\alpha_s^{(c)} = 0.7$ and (ii) hot ions with $T_-^{(h)} = 0.4\,\mathrm{eV}$ and $\alpha_s^{(h)} = 0.3$. This is a reasonable estimate, as can be concluded from Figs. 12(a) and 12(b). The model results in this case are given in Fig. 13(b). A space charge double layer is seen which is in agreement with the simulation. The distance from the ion sound velocity threshold to the wall is about $15\lambda_D = 0.45\,\mathrm{cm}$ which is comparable to 0.75 cm in the simulation. We have not seen the oscillation regime of the ion sound limitation, which, for oxygen, probably occupies a small region of the α_s, γ_-, γ_+ and ϵ parameter space.

A stronger double layer was observed in the case of $p = 10\,\mathrm{mTorr}$ ($n_0 = 3.2 \times 10^{20}\,\mathrm{m}^{-3}$) and $n_{e0} = 1.5 \times 10^{15}\,\mathrm{m}^{-3}$, shown in Fig. 14. In this case $\alpha_0 = 8$, $\alpha_s = 2$ and $\lambda/l = 0.2$. The point $\alpha_s/\alpha_0 = 0.25$, $\alpha_0 = 8$ falls between the two $\lambda/l = 0.2$ curves in Fig. 1. We have also run a case at the same pressure, but at higher power (higher n_{e0}) and observed that the charge double layers disappeared for $\alpha_0 < \alpha_{0\mathrm{cr}}$. The ion sound limitation condition, Eq. (31), and the existence of the double layers between the electronegative core and the electropositive halo is thus confirmed by the simulations.

VII. CONCLUSION AND DISCUSSION

Positive ions can be accelerated to the local ion sound velocity within the electronegative core. The ratio of the negative ion and electron densities in the discharge center α_0 must be larger than $\alpha_{0\mathrm{cr}}$ given by Eq. (32). The minimum value $\alpha_{0\mathrm{cr}}$ is inversely proportional to the ion mean free path, and therefore varies linearly with gas pressure. For $\alpha_0 > \alpha_{0\mathrm{cr}}$ the quasineutral electronegative solution breaks down. Assuming time-independent behavior, the quasineutral region can be matched to a solution in which space charge is included. Just beyond the transition the space charge region is similar in structure to a regular wall sheath, with the negative ions playing the role of electrons; the electron density is only slightly affected. As soon as the potential increases by a few times the negative ion temperature, the negative ion density becomes negligible, the positive ions become subsonic, and the structure of the space charge region changes depending on the values of α_s, the ratios of the negative ion to electron densities at the ion sound velocity threshold, $T_\pm/T_e$, and ϵ, the ratio of the local electron Debye length λ_D to the ion mean free path λ. Three regimes are identified, in order of decreasing α_s: the positive charge, charge double layer, and oscillation regimes. In the first regime, the charge region is positively charged and merges with the regular wall sheath. At lower α_s, the space charge density changes sign twice, forming a charge double layer between the electrone-

gative core and the wall sheath. In these two cases, the space charge region extends over a few electron Debye lengths. If α_s is reduced further, the potential, positive ion velocity, and positive ion and electron densities exhibit oscillatory behavior in space. The spatial period of the oscillation is on the order of the electron Debye length. If α_s is well below its value at the transition between the double layer and oscillation regimes, the plasma again becomes quasineutral downstream of the ion sound velocity threshold due to dissipative effects, and an electropositive halo can form. The nonneutral region is an internal sheath, with special characteristics, as described previously. The change in the electric potential across the internal sheath amounts to several times the negative ion temperature. This potential drop is sufficient to confine almost all negative ions to the electronegative core but has little effect on the electrons which are much hotter than the ions. The internal sheath extends over a length on the order of the ion mean free path.

Comparison of the theoretical model with the simulations demonstrates that the model predicts the existence of the various non-neutral regions qualitatively correctly. Of the three regimes named above, the positive charge and the charge double layer regimes were observed in the simulations. For the double layer regime, the structure of the nonneutral region in the simulation and in the model with the parameters taken from the simulation are similar. The oscillation regime has not been observed in the simulations, which may be due to its small size in the α_s, γ_-, γ_+ and ϵ parameter space, for oxygen. The size of the oscillation regime is smaller in a more collisional case (larger ϵ), and is smaller if high energy negative ions exist near the position of the ion sound velocity threshold.

In previous work[8] we used the ansatz that a small potential confined the negative ions to the core at the position where the positive ion drift velocity reached the local ion sound velocity. This resulted in truncated ion profiles with an abrupt density drop to the electropositive edge. Our results here support that ansatz. Abrupt transitions from the electronegative core to the electropositive edge studied in Refs. 5,6, and in our previous work[8] under the quasineutrality assumption, may be caused by the ion sound limitation and the consequential quasineutrality breakdown. However we also find that for the usual values of $T_\pm/T_e$ in a processing plasma, large values of α_s cannot be supported with an internal sheath. This result is not inconsistent with the range of plasma parameters explored in a previous paper,[8] but indicates that at the larger values of α_0 of the parameter space of Fig. 1, the internal sheath joins directly to the external sheath. As found in Ref. 11, in the equilibrium solutions with large α_0 and therefore large α_s, there is no significant quasineutral electropositive region, which is consistent with our present results. Since the edge region is generally small compared to an ionization length we expect our solution, which ignores ionization in the edge region, to be a reasonably accurate description of that region.

ACKNOWLEDGMENTS

The authors wish to acknowledge the support of NSF Grant No. ECS-9820836, California Industries, the Lam Research Corporation, and the State of California UC-SMART program under Contract No. 97-01.

[1] D. Bohm, *The Characteristics of Electrical Discharges in Magnetic Fields*, edited by A. Guthry and R. K. Wakerling (MacGraw–Hill, New York, 1949).
[2] M. A. Lieberman and A. J. Lichtenberg, *Principles of Plasma Discharges and Materials Processing* (Wiley, New York, 1994).
[3] R. L. F. Boyd and J. B. Thompson, Proc. R. Soc. London, Ser. A **252**, 102 (1959).
[4] L. D. Tsendin, Sov. Phys. Tech. Phys. **34**, 11 (1989).
[5] I. D. Kaganovich and L. D. Tsendin, Plasma Phys. Rep. **19**, 645 (1993).
[6] R. N. Franklin, P. G. Daniels, and J. Snell, J. Phys. D **26**, 1638 (1993); R. N. Franklin and J. Snell, *ibid.* **27**, 2102 (1994).
[7] A. J. Lichtenberg, V. Vahedi, M. A. Lieberman, and T. Rognlien, J. Appl. Phys. **75**, 2339 (1994).
[8] I. G. Kouznetsov, A. J. Lichtenberg, and M. A. Lieberman, Plasma Sources Sci. Technol. **5**, 662 (1996).
[9] B. M. Smirnov, *Physics of Weakly Ionized Gases* (Mir, Moscow, 1981).
[10] V. A. Godyak, *Soviet Radio Frequency Discharge Research* (Delphic Associates Inc., Falls Church, VA, 1986).
[11] A. J. Lichtenberg, I. G. Kouznetsov, Y. T. Lee, M. A. Lieberman, I. D. Kaganovich, and L. D. Tsendin, Plasma Sources Sci. Technol. **6**, 437 (1997).
[12] K.-U. Riemann, J. Phys. D **24**, 493 (1991).
[13] K.-U. Riemann, IEEE Trans. Plasma Sci. **23**, 709 (1995).
[14] K.-B. Persson, Phys. Fluids **5**, 1625 (1962).
[15] J. B. Thompson, Proc. Phys. Soc. London **73**, 818 (1959); G. L. Rogoff, J. Phys. D **18**, 1533 (1985); M. A. Lieberman and A. J. Lichtenberg, *Principles of Plasma Discharges and Materials Processing* (Wiley, New York, 1994).
[16] N. St. J. Braithwaite and J. E. Allen, J. Phys. D **21**, 1733 (1988).
[17] F. F. Chen, *Introduction to Plasma Physics and Controlled Fusion* (Plenum, New York, 1984).
[18] K.-U. Riemann and H.-P. van den Berg, Phys. Fluids B **3**, 1300 (1991).
[19] R. L. Burden and J. D. Faires, *Numerical Analysis* (PWS-KENT, Boston, 1989).
[20] R. P. Brinkmann, K. Loibl, and M. Kratzer, Efficient Two-Dimensional Simulation of Electronegative RF-Discharges in the Low Pressure Regime, 44th AVS National Symposium, 1997.
[21] J. P. Verboncoeur, M. V. Alves, V. Vahedi, and C. K. Birdsall, J. Comput. Phys. **104**, 321 (1993); V. Vahedi and M. Surendra, Comput. Phys. Commun. **87**, 179 (1995).
[22] E. A. Mason and E. W. McDaniel, *Transport Properties of Ions in Gases* (Wiley, New York, 1988).
[23] J. T. Gudmundsson, Ph.D. Dissertation, University of California, Berkeley, 1996.
[24] C.-F. Lin, *Advanced Control Systems Design* (Prentice–Hall, Englewood Cliffs, NJ, 1994).